J Therm Anal Calorim (2012) 107:395–405
DOI 10.1007/s10973-011-1581-y

Measuring the thermophysical properties of porous fibrous materials with a new unsteady-state method

Mingwei Tian · Sukang Zhu · Ning Pan

Received: 9 December 2010 / Accepted: 8 April 2011 / Published online: 1 May 2011

Abstract In this article, the authors first introduced a theoretical model dealing with unsteady-state heat conduction in porous fabric to assess the effects due to local convection during the testing. A few important issues are analyzed including the criterion for local thermal equilibrium in the fibrous materials and the confidence time region (t_{min}–t_{max}) during measuring process. The influence due to different heat source capacities can be ignored if the measuring time is greater than the minimum time duration t_{min}, yet the heat loss via outside surface becomes negligible if the testing duration is below the maximum allowable value t_{max}. Accordingly an apparatus that can simultaneously measure two thermophysical properties (the thermal conductivity k and thermal diffusivity a) of fibrous materials is developed in this study, which then leads to the determination of the volumetric capacity via $\rho C = k/a$. In order to minimize the influence of potential local micro heat convection and the contact resistance during heat transfer, some background, and stacking materials are adopted in the apparatus. The error range of the apparatus is estimated empirically based on the data from measuring some Perspex samples. Finally four kinds of polyester nonwoven fabrics with different porosities are tested using the device and the data analyzed and compared with theoretical predictions.

M. Tian · S. Zhu (✉) · N. Pan
Institute of Physics of Fibrous Soft Matters, Donghua University, Shanghai 200051, China
e-mail: zusukang@dhu.edu.cn

M. Tian
e-mail: tmw0303@mail.dhu.edu.cn

N. Pan
e-mail: npan@ucdavis.edu

M. Tian · N. Pan
Department of Biological and Agricultural Engineering, University of California, Davis, CA 95616, USA

Keywords Unsteady-state thermal test · Porous media · Theoretical analysis · Local heat convection · Local thermal equilibrium

List of symbols

a	Thermal diffusivity ($m^2\ s^{-1}$)
A_p	Pore surface area (m^2)
a_{sf}	The specific surface area of porous materials (m^{-1})
$F_n(x)$	Eigenfunction
h_e	Interstitial heat transfer coefficient ($Wm^{-2}\ K^{-1}$)
h	Thermometer's position (m)
k	Thermal conductivity [$Wm^{-1}\ K^{-1}$]
l	Fibrous material thickness in Fig. 1 and Fig. 3 (m)
Nn	Norm
Nu_{rh}	Nusselt number
$q(x, t)$	Heat flux (Wm^{-2})
r_h	Hydraulic radius, $\Delta V_p/\Delta A_p$ (m)
Sp	Sparrow number, $Sp = Nu_{rh}(k_f/k_e)(L/r_h)^2$
t	Time (s)
t_{max}	Confidence time region (s)
$T(x, t)$	Temperature excess (K)
T_0	Initial temperature (K)
$\vec{U}$	Velocity vector of fluid
V	Volume (m^3)
V	Heat transfer coefficient ($Wm^{-2}\ K^{-1}$)
X	Space coordinate in x direction (m)

Greek symbols

ε	Porosity of fibrous material $\varepsilon = V_f/V$
γ_n	Eigenvalue
ρC	Heat capacity/unit volume ($Jm^{-3}\ K^{-1}$)
τ_t	Lag time of the temperature gradient (s)
τ_q	Lag time of the heat flux (s)
τ_e	$\tau_e = (1-\varepsilon)\langle \rho C \rangle^s \tau_t / \rho C$

Subscripts

b Background material
f Fluid phase
s Solid phase

Introduction

Porous fibrous materials exhibit complex behaviors in mechanical [1, 2], thermal [3, 4], optical [5, 6], and electrical [7] processes. Recently, Pan [3, 8, 9] proposed a new concept "fibrous soft matter" to represent the fibrous materials by highlighting their multiphase nature and variable properties. In thermal aspect, porous fibrous materials are widely used for heat protection applications such as in fire-fighting suit [10] and in building thermal insulation [11], and the desirable thermophysical properties of the fibrous materials are the essential reason for their wide acceptance, so measuring and evaluating such properties are critical for material selection and design.

Fibrous materials as multi-phase media consist mainly of fiber and moistured air. Therefore, the heat transfer process in such materials is very complex, either in single heat conduction where multiple components of fiber, moisture, and air and intricate interfacial phenomena between them are involved, or much more so in a combined process including heat conduction, convection, and radiation. Although, researchers [12–18] have developed certain theories on heat transfers in porous multi-phase materials and established the heat transfer equations at the representative elementary volume (REV) scales that can explicitly describe single or combined heat transfer mechanisms in such porous materials, the structural flexibility and compressibility of fibrous materials have posed new challenges to the validity of those theories.

In experimental approaches, at present, the steady-state methods [19, 20] such as guarded hot plate (GHP) and the dynamic methods [21–24] are the dominant tools for homogenous materials thermophysical measurement, GHP is the most frequently used method for fibrous materials, but several factors significantly influence the test accuracy and reliability. First, long time is required for fibrous material to reach steady-state conditions before measurements can be taken, but such long time leads to evaporation of the moisture within and thus significantly alters the material properties. Also most established methods are developed for measuring the thermal conductivity only, and unable to test other important parameters such as the thermal diffusivity and volumetric capacity which are critical in accounting for the transient behaviors, as elucidated in more detail later in this article. Next, even at the steady-state, heat transfer in a fibrous sample usually takes place in a combined form of heat conduction, convection, and radiation during a test because the temperature difference between the two side of the sample is normally kept at 10–20° in such measurement schemes [25, 26], too high to neglect the convection and radiation, the so-called thermal conductivity thought tested is actually a more complex parameter. Finally it is not easy to maintain such constant temperature difference between the sample during test due to the inevitable fluctuations in the external environment [27].

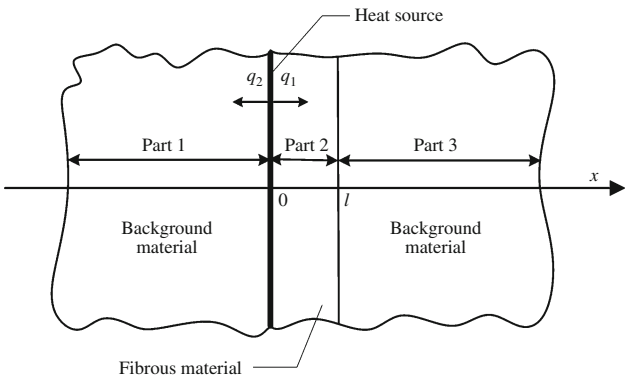

Fig. 1 The model of the unsteady-state method

To overcome the problems, Kubicar et al. [28, 29] proposed a step-wise method to quickly measure the thermal properties of continuous media based on the unsteady-state heat conduction theories. Zuo et al. [30] from the group adopted this method for fibrous materials and set up an apparatus in which the sample size is properly determined to minimize the test errors resulted from the boundary heat loss [31]. However, this method suffers other discrepancies because of the interference of the thermal contact resistance caused by having to use multi-layer stacking samples and the associated residual local natural convection.

In this article, the authors developed a theoretical model dealing with the multi-layer unsteady-state heat conduction to assess the effect due to local convection during the testing. A few important issues are then analyzed including the criterion of local thermal equilibrium (LTE) in fibrous materials and the confidence time region ($t_{\min}$–$t_{\max}$) during the measuring process. Accordingly an unsteady-state apparatus that can simultaneously measure two thermophysical properties (the thermal conductivity k, thermal diffusivity a), then the volumetric capacity using $\rho C = k/a$ is introduced in this article. In order to minimize the influence of potential local micro heat convection and contact resistance during heat transfer, some background, and stacking materials are adopted in the apparatus. The error range of the apparatus is estimated empirically based on the data from measuring some Perspex samples. Finally four kinds of PET nonwoven fabrics with different

densities are tested using the device and the data analyzed and compared with theoretical predictions.

Heat transfer process in porous fibrous materials

Heat transfers dealt with in this article focus on the low heat flux density and small temperature gradient, so that the heat radiation can be ignored because of its marginal impact. According to the theories of heat conduction and convection in fibrous materials, the governing equations of such heat transfers are as follows [12, 13]:

$$\varepsilon\langle\rho C\rangle^{\mathrm{f}}\frac{\partial T_{\mathrm{f}}(x,t)}{\partial t}+\langle\rho C\rangle^{\mathrm{f}}\overrightarrow{U}*\nabla T_{\mathrm{f}} = \varepsilon\nabla*(k_{\mathrm{f}}\nabla T_{\mathrm{f}})+h_{\mathrm{e}}a_{\mathrm{sf}}(T_{\mathrm{s}}-T_{\mathrm{f}}) \tag{1a}$$

$$(1-\varepsilon)\langle\rho C\rangle^{\mathrm{s}}\frac{\partial T_{\mathrm{s}}(x,t)}{\partial t}=(1-\varepsilon)\nabla*(k_{\mathrm{s}}\nabla T_{\mathrm{s}})-h_{\mathrm{e}}a_{\mathrm{sf}}(T_{\mathrm{s}}-T_{\mathrm{f}}) \tag{1b}$$

where, $T_{\mathrm{f}}(x, t)$ for the fluid phase and $T_{\mathrm{s}}(x, t)$ for the solid are the two volume averaged temperatures over the representative element volumes associated with each point regardless of whether that point is located in the solid phase, fluid phase, or on the interface. Both of them can be defined as in Ref. [32]:

$$T_{\mathrm{f}}(x,t)=\frac{1}{V_{\mathrm{f}}}\int_{V_{\mathrm{f}}}T\mathrm{d}V \qquad T_{\mathrm{s}}(x,t)=\frac{1}{V_{\mathrm{s}}}\int_{V_{\mathrm{s}}}T\mathrm{d}V$$

where V_{f} and V_{s} are the volumes of fluid and solid phases within the averaging volume V. Based on the energy conversion $Q = Cm\Delta T$, the heat exchange between the solid and fluid in the fibrous material system can be shown as:

$$\langle\rho C\rangle^{\mathrm{f}}\Delta V_p\frac{\partial T_{\mathrm{f}}}{\partial t}=h_{\mathrm{e}}\Delta A_p(T_{\mathrm{s}}-T_{\mathrm{f}}) \tag{1c}$$

where $\varepsilon = V_{\mathrm{f}}/V$ is the porosity, $\langle\rho C\rangle^{\mathrm{f}}$,$\langle\rho C\rangle^{\mathrm{s}}$, k_{f} and $k_{\mathrm{s}}$are the volumetric capacity and thermal conductivity of the fluid and solid, respectively; h_{e} is the interstitial heat transfer coefficient between the two phases; $\overrightarrow{U}$is the fluid velocity vector; a_{sf} is the specific surface area of the porous materials, ΔV_{p} and ΔA_{p} are the volume and surface area of a mean pore. So the heat transfer equations set for the fibrous material can be obtained from Eqs. 1a–c as:

$$\begin{cases}(1-\varepsilon)\langle\rho C\rangle^{\mathrm{s}}\frac{\partial T_{\mathrm{s}}}{\partial t}+\varepsilon\langle\rho C\rangle^{\mathrm{f}}\frac{\partial T_{\mathrm{f}}}{\partial t}+\langle\rho C\rangle^{\mathrm{f}}\overrightarrow{U}*\nabla T_{\mathrm{f}} \\ \quad=\varepsilon\nabla*(k_{\mathrm{f}}\nabla T_{\mathrm{f}})+(1-\varepsilon)\nabla*(k_{\mathrm{s}}\nabla T_{\mathrm{s}})\end{cases} T_{\mathrm{s}}(x,t)=T_{\mathrm{f}}(x,t)+\tau_t\frac{\partial T_{\mathrm{f}}(x,t)}{\partial t} \tag{2}$$

where parameter $\tau_t = \Delta V_p\langle\rho C\rangle^{\mathrm{f}}/\Delta A_p h_{\mathrm{e}} = r_{\mathrm{h}}\langle\rho C\rangle^{\mathrm{f}}/h_{\mathrm{e}}$, with $r_{\mathrm{h}} = \Delta V_p/\Delta A_p$ as the pore hydraulic radius. The lag time τ_t is the phase-lag in the temperature gradient. Once the parameters in Eq. 2 are known under given initial and boundary conditions, the heat transfer process in fibrous materials can be solved.

Further, when the local temperatures of the adjacent fluid and solid phases are equal to each other, i.e., $T_{\mathrm{f}}(x, t) = T_{\mathrm{s}}(x, t)$, the lag time $\tau_t \to 0$. The heat transfer process is then considered to have reached the local thermal equilibrium (LTE), and the heat transfer process in Eq. 2 can be simplified into a one-equation model:

$$\rho C\frac{\partial T}{\partial t}+\langle\rho C\rangle^{\mathrm{f}}\overrightarrow{U}*\nabla T=\nabla*(k\nabla T) \tag{3}$$

where $k=\varepsilon k_{\mathrm{f}}+(1-\varepsilon)k_{\mathrm{s}}$, $\rho C=\varepsilon\langle\rho C\rangle^{\mathrm{f}}+(1-\varepsilon)\langle\rho C\rangle^{\mathrm{s}}$ are, respectively, the thermal conductivity and volumetric capacity of the fibrous material.

In most practical conditions, the difference between temperatures T_{s} and T_{f} of the two phases is negligible so that the heat transfer in fibrous materials can be viewed as at LTE (see more in The criterion of local thermal equilibrium (LTE)), Eq. 3 can be applied directly to describing such heat transfer process. Three parameters (the thermal conductivity k, volumetric capacity ρC, and the fluid velocity $\overrightarrow{U}$) collectively determine the heat transfer process according to Eq. 3. Therefore, measurement of the thermophysical properties (k and ρC) is a foundational and important work. Considering most existing instruments focus on measuring the thermal conductivity k only, an apparatus specially designed for simultaneously testing both the thermal conductivity k and the volumetric capacity ρC is introduced below.

Theoretical model and measuring apparatus

The measurement principle

The illustration of the proposed new unsteady-state test method is shown in Fig. 1. Part 1 is the added background material with infinite thickness; Part 2 is the fibrous material (thickness l) under testing, and Part 3 consists of the same background material as Part 1. The initial temperature $T_0 = 0$ at $t = 0$ is the same everywhere in the

model. At time $t > 0$, the heat source releases a constant heat flux $q_0 = q_1 + q_2$, with q_1 to one side and q_2 to the other as shown.

The governing equations of the temperatures T_1 (in Part 1), T_2 (in Part 2), T_3(in Part 3) in the system are shown as:

$$a_b\frac{\partial^2 T_1}{\partial x^2} = \frac{\partial T_1}{\partial t} \qquad -\infty \le x \le 0 \tag{4a}$$

$$a\frac{\partial^2 T_2}{\partial x^2} = \frac{\partial T_2}{\partial t} \qquad 0 \le x \le l \tag{4b}$$

$$a_b\frac{\partial^2 T_3}{\partial x^2} = \frac{\partial T_3}{\partial t} \qquad l \le x \le +\infty \tag{4c}$$

The initial conditions ($t = 0$) are given by:

$$T_1(x,t)|_{t=0} = T_2(x,t)|_{t=0} = T_3(x,t)|_{t=0} = 0 \tag{5a}$$

The outer boundary ($x \to \pm\infty$) conditions are:

$$T_1(x,t)|_{x\to-\infty} = T_3(x,t)|_{x\to+\infty} = 0 \tag{5b}$$

The inner boundary ($x = 0$ and $x = l$) conditions:

$$T_1(x,t)|_{x=0} = T_2(x,t)|_{x=0} \tag{5c}$$

$$q_2 = k_b\frac{\partial T_1(x,t)|_{x=0}}{\partial x} \tag{5d}$$

$$q_1 = -k\frac{\partial T_2(x,t)|_{x=0}}{\partial x} \tag{5e}$$

$$T_2(x,t)|_{x=l} = T_3(x,t)|_{x=l} \tag{5f}$$

$$k\frac{\partial T_2(x,t)|_{x=l}}{\partial x} = k_b\frac{\partial T_3(x,t)|_{x=l}}{\partial x} \tag{5g}$$

The temperature distribution in each part can thus be derived under given conditions by solving the above corresponding equations using, for instance, the Laplace methods [33]:

$$T_1(x,t) = \frac{2q_0}{k^+}\sum_{n=0}^{\infty}\left(\frac{k^-}{k^+}\right)^{2n}\sqrt{t}\left[i\Phi_c\left(\frac{-x+2nl\sqrt{a_b/a}}{2\sqrt{a_b t}}\right) - \frac{k^-}{k^+}i\Phi_c\left(\frac{-x+(2n+1)l\sqrt{a_b/a}}{2\sqrt{a_b t}}\right)\right] \quad -\infty \le x \le 0 \tag{6a}$$

$$T_2(x,t) = \frac{2q_0}{k^+}\sum_{n=0}^{\infty}\left(\frac{k^-}{k^+}\right)^{2n}\sqrt{t}\left[i\Phi_c\left(\frac{x+2nl}{2\sqrt{at}}\right) - \frac{k^-}{k^+}i\Phi_c \times\left(\frac{-x+(2n+1)l}{2\sqrt{at}}\right)\right] \qquad 0 \le x \le l \tag{6b}$$

$$T_3(x,t) = \frac{2q_0}{k^+}\left(1-\frac{k^-}{k^+}\right)\sum_{n=0}^{\infty}\left(\frac{k^-}{k^+}\right)^{2n}\sqrt{t}\,i\Phi_c \times\left(\frac{x-l+(2n+1)l\sqrt{a_b/a}}{2\sqrt{a_b t}}\right) \qquad l \le x \le +\infty \tag{6c}$$

where $k^+ = k_b/\sqrt{a_b} + k/\sqrt{a}$,$k^- = k_b/\sqrt{a_b} - k/\sqrt{a}$, k, a and k_b, a_b are thermal conductivity and thermal diffusivity of the fibrous material and the background material, respectively, in addition to $i\Phi_c(u) = \pi^{-1/2}\exp(-u^2) - uErfc(u)$.

The measuring apparatus

According to the analysis above, a test apparatus is set up in the lab as illustrated in Fig. 2. The apparatus includes three parts: the sample heating unit (SHU), the data acquisition unit (DAU), and a computer for data analysis.

Thickness of the fibrous material is usually too small to reach the critical thicknesses 0.002–0.01 m [29, 30, 34]. So, to meet the thickness requirement, the sample-box (total thickness h) is composed of the fibrous material of thickness l, and the stacking material of the same type as the background ones. Therefore, the SHU unit consists of the sample-box, background material, heating circuit, and preheat circuit (used to preheat and stabilize the power source to avoid voltage surge when initiating the heat circuit). A membrane heat source in the heating circuit is a flexible nickel foil film 0.1 × 0.1 m with an electric resistant (18.6 Ω) to match the preheat resistant required by the preheat circuit and its thickness is less than 0.1 mm. The area size of the sample-box and background material are both 0.1 × 0.1 m, the same as the heat source, and the background material thickness are set as 0.05 m in order to minimize the contact thermal resistance and boundary heat loss. The combined influence of heat source capacity and boundary heat loss are discussed in a later section.

DAU is made up of both the data acquisition and a thermometer placed at the centerline between the sample-box and the background surface so that the sample-box temperature can be measured and recorded by the computer at a sampling frequency 4 Hz.

The stacking material is needed when the thickness of fibrous material is thinner than 0.002 m. In this case, the temperature equation at the thermometer's location ($x = h > l$) can be derived from Eq. 6c as:

$$T_3(h,t) = \frac{2q_0}{k^+}\left(1-\frac{k^-}{k^+}\right)\sum_{n=0}^{\infty}\left(\frac{k^-}{k^+}\right)^{2n}\sqrt{t}\,i\Phi_c \times\left(\frac{h-l+(2n+1)l\sqrt{a_b/a}}{2\sqrt{a_b t}}\right) \qquad l < h < +\infty \tag{7}$$

When the thickness of fibrous material is in the range 0.002–0.01 m, there is no need for the stacking material, so $h = l$ and Eq. 7 is reduced into:

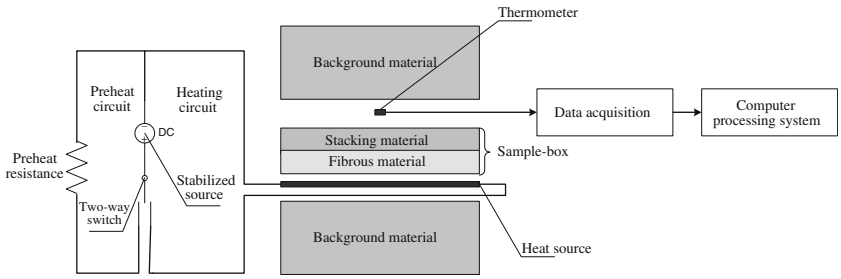

Fig. 2 The schematic diagram of measuring apparatus

$$T_3(h,t) = \frac{2q_0}{k^+}\left(1-\frac{k^-}{k^+}\right)\sum_{n=0}^{\infty}\left(\frac{k^-}{k^+}\right)^{2n}\sqrt{t}\,i\Phi_c \times\left(\frac{(2n+1)l}{2\sqrt{at}}\right) \qquad h=l \tag{8}$$

The thermophysical properties can be firstly estimated from the experimental temperature curves using Eqs. 7–8 by data-fitting methods [29, 30] in such steps: choosing appropriate time window and interval in the temperature curve and then dividing this curve into n time windows; in each time window, the thermal conductivity k_p ($p = 1, 2,\ldots, n$) and thermal diffusivity a_p can be derived from Eqs. 7–8 by the least square methods and then the volumetric capacity calculated as $\rho C_p = k_p/a_p$; and then, the obtained values of the three properties (k_p, a_p, and ρC_p) are, separately, plotted along with the mean time of each corresponding time window, and then the confidence time region ($t_{\min x} \sim t_{\max}$) of each curve can be determined (see details in The determination of confidence time region ($t_{\min} \sim t_{\max}$) below); finally the average values over this region ($t_{\min x} \sim t_{max}$) are the results of the thermophysical properties of the sample tested.

Important parameters

To assure the reliability of the data obtained, a few issues have to be settled. First, it has to be sure the measurement is done when the multi-phase sample tested is under local thermal equilibrium. Also the heat losses due to the different heat source capacity and limited system size, as opposed to the semi-infinite assumption implied in all the theories used, are within allowable range. In addition, a heat source with proper heat flux is used in the test so that the potential local heat convection becomes negligible.

The criterion of local thermal equilibrium (LTE)

The solid and fluid phases in a fibrous material exchange heat during the heat conduction processing and such exchange determines the condition of local thermal equilibrium (LTE). Once at LTE, the heat exchange between the two phases reaches a dynamic equilibrium and the temperatures of the two phases become equal, $T_s = T_f$. At this moment, a fibrous material can be treated as equivalent as a thermally homogenous material in macro-scale, so that the heat conduction in the fibrous material can be described by Eqs. 4–8 and these equations become valid for the apparatus.

As shown in Fig. 3, the fibrous material (thickness l) is in close contact with a planar heat source at $x = 0$ so that $x = l$ can be treated as an adiabatic surface. When $t > 0$, the heat source heats up the fibrous material with a constant heat flux. According to Eq. 2: $T_s(x,t) - T_f(x,t) = \tau_t \frac{\partial T_f(x,t)}{\partial t}$, i.e., the temperature difference between the solid and fluid $T_s - T_f$ is the product of both the lag time τ_t and the temperature change rate $\partial T_f/\partial t$. Here τ_t is the intrinsic property of the fibrous material, but $\partial T_f/\partial t$ relates to the boundary conditions and reaches the maximum value at the adiabatic surface. Therefore at the adiabatic surface, the temperature difference $T_s - T_f$ achieves the maximum and the system deviates most from the LTE. So we can adjust the adiabatic surface ($x = l$) to examine the conditions for reaching the LTE state.

The general solution of heat transfer equations Eq. 2 for non-flow or with negligible flow are given in Refs. [14, 15], so the fluid phase temperature equation of the sample in Fig. 3 can be derived based on the given boundary conditions (the planar heat source $S(x', t) = q_0\ \delta(x-0)$, where the Dirac delta function $\delta(x-0) = 1$ when $x = 0$, otherwise $\delta(x-0) = 0$):

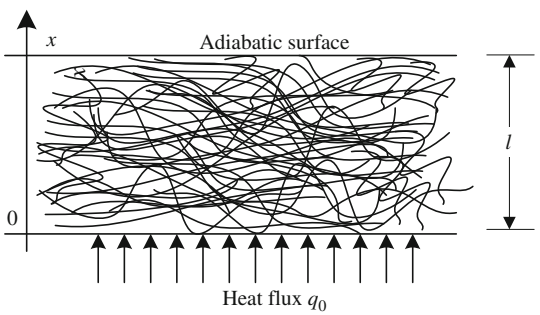

Fig. 3 The schema of the fibrous materials

$$T_{\mathrm{f}}(x,t)=\sum_{n=0}^{\infty}\frac{q_0\mathrm{F}_n(x)}{\rho C N_n(\tau_{\mathrm{q}}+\tau_{\mathrm{e}})\omega_n}\times\left[\frac{-2\omega_n+(\omega_n+a_n)e^{(\omega_n-a_n)t}+(\omega_n-a_n)e^{-(\omega_n+a_n)t}}{2(\omega_n^2-a_n^2)}\right] \tag{9}$$

where the eigenfunctions for the adiabatic boundary conditions are $\mathrm{F}_n(x)=\cos(n\pi x/l)$ that yield the eigenvalues $\gamma_n=(n\pi/l)^2k_{\mathrm{e}}/\rho C$ for $n=0,\ 1,\ 2,\ldots$, and the Norm is $Nn=l$ $(n=0)$, and $Nn=l/2$ $(n>0)$. Other parameters appearing in Eq. 9 are:

$$a_{\mathrm{m}}=\frac{1}{2(\tau_{\mathrm{q}}+\tau_{\mathrm{e}})}(1+\gamma_n\tau_t)\,\omega_n=\gamma_n\sqrt{\left[1-\frac{\tau_t}{2(\tau_{\mathrm{q}}+\tau_{\mathrm{e}})}-\frac{1}{2\gamma_n(\tau_{\mathrm{q}}+\tau_{\mathrm{e}})}\right]^2-\left|1-\frac{\tau_t}{(\tau_{\mathrm{q}}+\tau_{\mathrm{e}})}\right|}$$

where τ_{q} is interpreted as the relaxation time resulting from the fast-transient effect due to thermal inertia and is named as the phase-lag of the heat flux, and can be expressed as $\tau_{\mathrm{q}}\approx C_{\mathrm{s}}R_{\mathrm{c}}\Delta V_{\mathrm{s}}/\Delta A_{\mathrm{s}}$ [18, 35]. τ_t is a parameter to describe the time delay in temperature gradient across the differential phase defined in Eq. 2 and can be expressed in terms of the dimensionless parameter Sp as $\tau_t=l^2\langle\rho C\rangle^{\mathrm{f}}/(kSp)$, where the Sparrow number $Sp=hl^2/(kr_{\mathrm{h}})$ as defined in Refs. [14] which can also be rewritten as the function of the Nusselt number as $Sp=Nu_{\mathrm{rh}}(k_{\mathrm{f}}/k)(l/r_{\mathrm{h}})^2$,where $Nu_{\mathrm{rh}}=hr_{\mathrm{h}}/k_{\mathrm{f}}$. The third delay time τ_{e} can then be defined as $\tau_{\mathrm{e}}=(1-\varepsilon)\langle\rho C\rangle^{\mathrm{s}}\tau_t/\rho C$.

According to Eqs. 2 and 9, the dimensionless temperature curves of the fluid T_{f} and solid T_{s} are plotted against the dimensionless time at/l^2 in Fig. 4, as a function of the Sp values. The authors can find that, for a given material, the solid and fluid temperatures are closer with a greater Sp; and once Sp is beyond a certain level ($Sp>500$ in this case), the temperature difference between two phases can be ignored and the heat transfer can be deemed at the LTE condition. So the Sp number is an important parameter in verifying the existence of the local thermal equilibrium in the porous materials.

For fibrous materials, their Sp values can be calculated from $Sp=Nu_{\mathrm{rh}}(k_{\mathrm{f}}/k)(l/r_{\mathrm{h}})^2$, where $Nu_{\mathrm{rh}}\approx 1$ for fibrous materials with various pore shapes, k_{f} and k are the thermal conductivities of still air (0.03 $\mathrm{Wm^{-1}\,K^{-1}}$, [36]) and fibrous materials (0.05–0.5 $\mathrm{Wm^{-1}\,K^{-1}}$ [37]), respectively. The thicknesses of the fibrous materials l are around 0.03–0.1 m for most applications. In addition, the hydraulic radius $r_{\mathrm{h}}=\Delta V_{\mathrm{p}}/\Delta A_{\mathrm{p}}=(4\pi r^3/3)/(4\pi r^2)=\mathrm{r}/3$ and the pore diameter r vary over 50–500 μm [38]. Thus, the estimated range for Sp values is 1.1×10^3–1.25×10^5. Consequently T_{f} and T_{s} in the fibrous materials are nearly equal such that the system is at the LTE condition. Equations 4–8, as the theoretical basis, can be used for this apparatus.

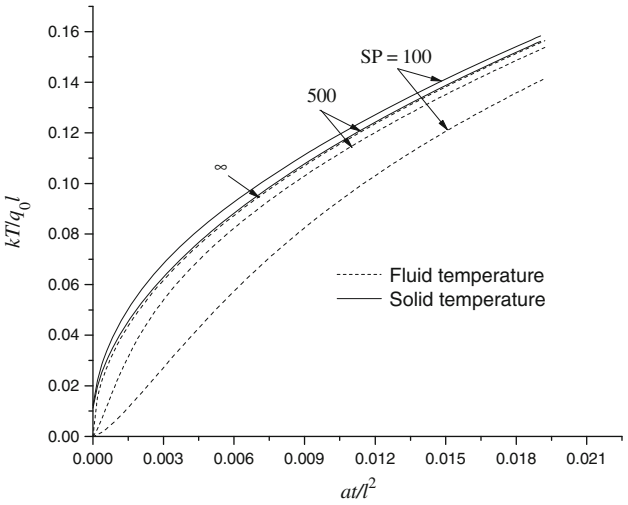

Fig. 4 The fluid and solid dimensionless temperature curve with three different Sp values ($Sp=100$, 500, and ∞) at $x=0$ when the sample was chosen as $l=0.01$ m, $k_{\mathrm{f}}=0.025$ $\mathrm{Wm^{-1}\,K^{-1}}$, $\rho C_{\mathrm{f}}=1.21\times10^3\mathrm{J\,m^{-3}\,K^{-1}}$, $k_{\mathrm{s}}=0.1$ $\mathrm{Wm^{-1}\,K^{-1}}$, $\rho C_{\mathrm{s}}=6\times10^5\mathrm{J\,m^{-3}\,K^{-1}}$, the porosity $\varepsilon=0.7$ and $q_0=100$ $\mathrm{Wm^{-2}}$

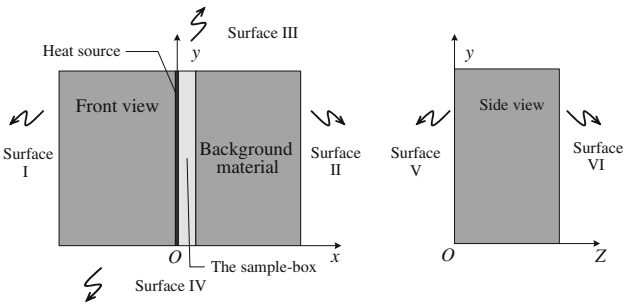

Fig. 5 The schematic diagram of the actual apparatus

The determination of confidence time region ($t_{\min}$–$t_{\max}$)

In the set-up in Fig. 1, the background materials are assumed as a semi-infinite slab. Also an ideal heat source is assumed with a negligible thickness and made of the same material as the samples tested [34]. This is clearly not the case in the actual apparatus shown in Fig. 5, where all the outside surfaces (Surfaces I–VI) directly contact and exchange the heat with the surrounding atmosphere. Meanwhile the heat source owns considerable thickness with different thermophysical properties from the samples. According to Ref. [39], the heat loss via outside surface becomes negligible if the testing duration is below a critical value $t_{\max}$. On the other hand, the influence due to the different heat source capacities can be ignored if the measuring time is greater than another time duration $t_{\min}$. It

Table 1 Thermophysical properties of sample and background material

Parameter	k/Wm^{-1} K^{-1}	$a \times 10^{-6}$/m^{2}s^{-1}	k_b/Wm^{-1} K^{-1}	$a_b \times 10^{-6}$/m^2 s^{-1}
Range	0.03–0.3	0.1–1	0.03–0.6	0.1–2
Default Value	0.15	0.5	0.3	1

was thus define (t_{min}–t_{max}) as the confidence time region, satisfying the equation:

$$\left|\frac{k_E^{t_{min}} - k_T}{k_T}\right| = \left|\frac{k_E^{t_{max}} - k_T}{k_T}\right| = 1\% \quad (10)$$

where $k_E^{t_{min}}$ and $k_E^{t_{max}}$ are the thermal conductivities, estimated from the temperature curve thus including the heat source effect and boundary heat loss; and the constant k_T represents the theoretical value without the errors.

All the calculations are done using the software package ANSYS, establishing a 3-D model of SHU in Fig. 5 and choosing the Solid 90 as the space element. The properties of the sample and background material are listed in Table 1, while the thermal conductivity and thermal diffusivity of the heat source are set as 59.5 Wm^{-1} K^{-1} and 1.5×10^{-5} m^2 s^{-1}, respectively. The thickness of the heat source membrane, the sample and background material is set as 0.0001, 0.005, and 0.05 m, respectively, with the same area size 0.1 × 0.1 m. The contact thermal resistance between them is ignored, and the heat flux from the heat source is $q_0 = 100$ Wm^{-2} and the heat transfer coefficient with the surrounding air is set as $v = 10$ Wm^{-2} K^{-1}.

During the calculations, when changing the value of one parameter within its range, others are fixed at the default values in the above table. First record the temperature data at the centerline of the interface between the sample and the background materials; then utilize the data to fit parameter k_E^t by Eqs. 7–8, and determine the confidence time region (t_{min}–t_{max}) from Eq. 10. Through a series of calculation iterations, the temperature data were found to converge to an exactly value, when the mesh size is smaller than 1×10^{-5} m and time interval is shorter than 0.01 s.

In Fig. 6, corresponding to each curve, the region (t_{min}–t_{max}) data are plotted against a chosen parameter while others kept constant. For instance, it is shown that the t_{max} values increase with either the thermal diffusivity a of the sample or the thermal conductivity k_b of the background material while decrease with the sample thermal conductivity k and the diffusivity a_b of the background material. Whereas the t_{min} values increase with the thermal conductivity k, the diffusivity a of the sample and a_b of the background material but decrease with k_b of the background material. In other words, for given samples, selecting a background material with large thermal

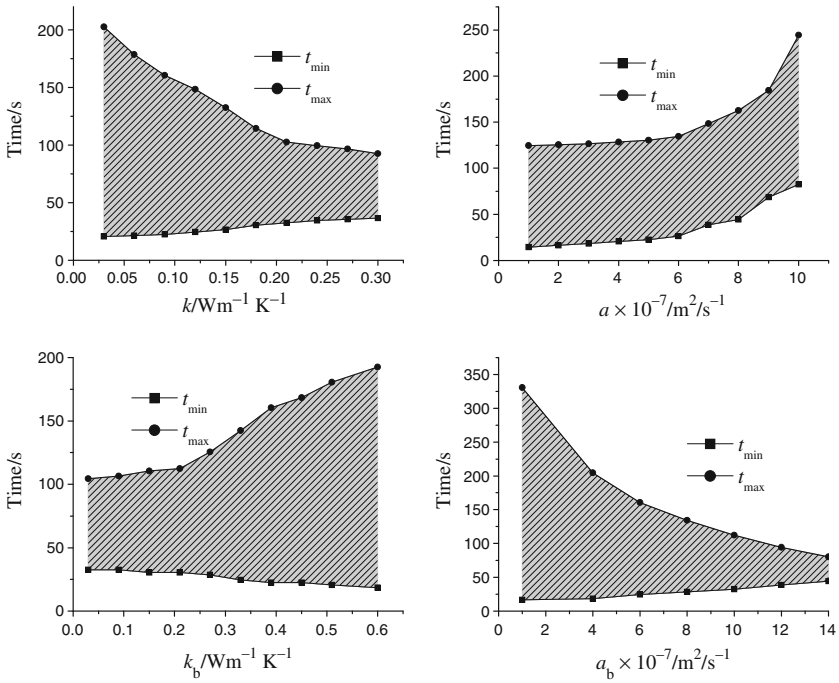

Fig. 6 The effect of thermophysical properties of the sample and background material on $t_{min} \sim t_{max}$

conductivity k_b yet small diffusivity a_b can expand the confidence time region (t_{min}–t_{max}). Thus, for the apparatus, Perspex is chosen as the background material for its desirable combination in thermophysical properties.

Once Perspex is chosen as the background material, the range of confidence time region (t_{min}–t_{max}) is determined by k and a of the sample materials, and is found to be 30–210 s for most fibrous materials.

Choosing the heat flux of the heat source

Natural heat convection in fibrous materials may be excited when a large heat flux goes through it. According to Ref. [30], after tests at different heat flux values, it was found that when the heat flux of heat source is smaller than 100 Wm^{-2}, heat conduction becomes the dominant heat transfer form in the fibrous material. Therefore, the heat flux of the apparatus is set at 100 Wm^{-2}.

Overall accuracy of the measuring apparatus

In order to verify the reliability of this apparatus, the Perspex as a testing material is measured using this apparatus. Its actual thermophysical properties are given in Ref. [29] (thermal conductivity 0.187 Wm^{-1} K^{-1}, thermal diffusivity 1.08×10^{-7} m^2 s^{-1}, and volumetric capacity 1.75×10^6 J m^{-3} K^{-1}). The data were averaged over three testing repeats and the relative errors (|measured value−actual value|/actual value) calculated shown in Table 2. The relative errors vary from 1.71 to 3.72% so the measured thermal properties for the Perspex agree well with the reference values. The reliability of the apparatus for solid homogenous materials is thus demonstrated.

Applying the apparatus to fibrous materials

The authors selected four kinds of PET (polyester) nonwoven fabrics as the samples to measure the thermophysical properties with the apparatus and their basic parameters are shown in Table 3 where Fabrics A-I and B-I require the stacking material (Perspex 0.002 m) to fill the sample-box to reach the desirable thickness for using Eq. 7, whereas A-II and B-II, already with proper thickness, can be measured directly without the stacking material and calculate the results using Eq. 8.

Table 2 Measured value and relative error of the Perspex samples

	k_b/Wm^{-1} K^{-1}	$a_b \times 10^{-7}$/ m^2 s^{-1}	$\rho_b C \times 10^6$/ J m^{-3} K^{-1}
Measure value	0.193	1.12	1.72
Relative error (%)	3.23	3.72	1.71

Table 3 Basic physical parameters of samples

Number	Thickness/ m	Bulk density/ kg m^{-3}	Surface density/ kg m^{-2}	Porosity/ %*
A-I	0.002	198.83	0.398	80.2
A-II	0.004	198.83	0.795	80.2
B-I	0.002	18.38	0.037	98.1
B-II	0.004	18.38	0.074	98.1

* Porosity is derived from $\varepsilon = (1-\rho_{bulk}/\rho_{particle}) \times 100\%$

Each sample was tested in five repeats this round under the same standard experimental conditions of temperature 20 °C and relative humidity 65%. It was first calculated the parameters k and a from Eqs. 7 and 8 using the recorded temperature data. The same parameters were also obtained experimentally by taking the average values in the confidence time region. Figure 7a and b shows the calculated and experimental values of thermal conductivity for sample AI: Fig. 7a is the curve from the calculations by ANSYS considering both the heat source effect and the heat loss, while Fig. 7b provides the experimental values measured using the present apparatus. Clearly both curves match with each other very well within the confidence time region around 36.5–192.5 s. The confidence time regions determined for other three types samples [AII, BI, and BII] are: 34.5–190.5 s, 30.5–200.5 s, and 30.5–202.5 s, respectively.

The actual results are illustrated in Fig. 8 and also summarized in Table 4. First it can be seen that, as shown in both cases with and without the stacking material, the test reproducibility is satisfactory with the confidence interval 5% for thin (A-I and B-I) and thick (A-II and B-II), or low density (B-I and B-II), and high density samples (A-I and A-II).

From the data we also find that the high-density samples (A-I, A-II) possess greater thermal conductivity and volumetric heat capacity but smaller thermal diffusivity, as dictated by $\rho C = k/a$, than the low density ones (B-I and B-II). Such influence of material density on the thermal properties derived is relatively easy to explain in the samples used here where the air and PET fibers are mixed homogenously and the heat transfer is at LTE condition so that the authors can use an effective hypothetical simple material (homogenous with single component and phase) to represent the original multiphase sample. Using the thermal properties of each component (air and PET fiber) listed in Table 5 with data drawn from Refs. [40, 41], the tested results in Table 4 are in fact consistent with the predictions given by Wang and Pan in [3] that with the increase of PET content, the thermal conductivity (k) and

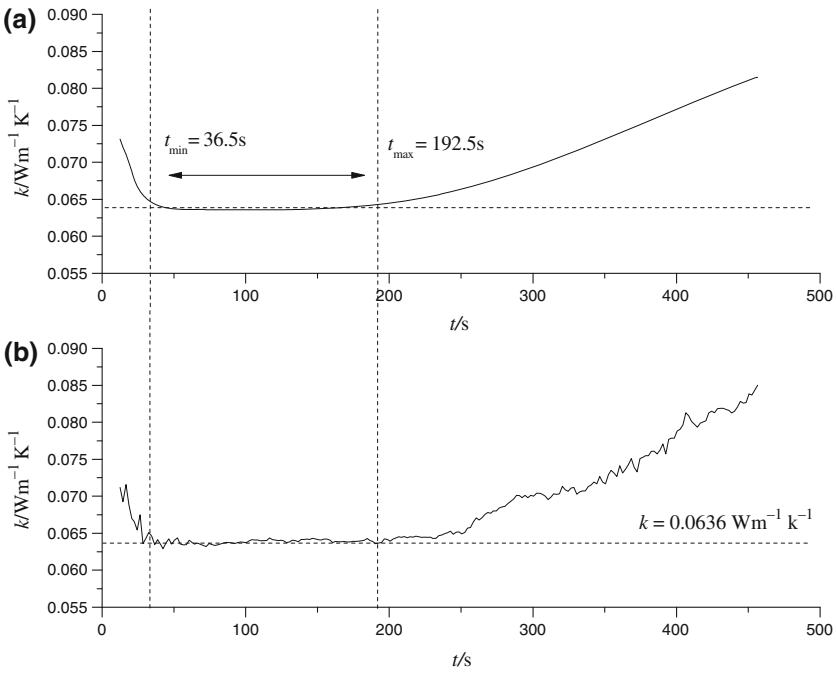

Fig. 7 **a** The calculated values for sample AI by ANSYS (sample thickness 0.002 m, $k = 0.636$ Wm^{-1} K^{-1}, $a = 1.46 \times 10^{-7}$ m^2 s^{-1} and stacking Perspex thickness 0.003 m, background Perspex 0.05 m). **b** The experimental results measured using the apparatus

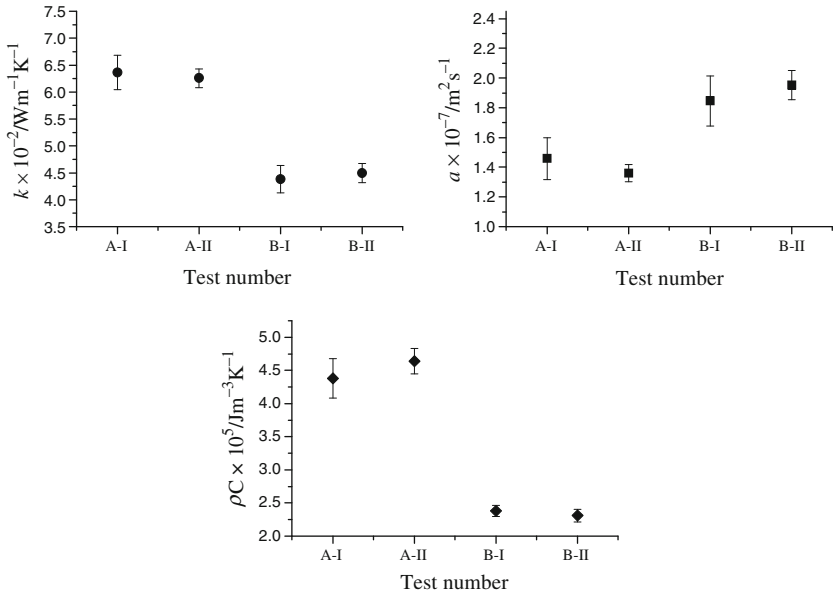

Fig. 8 The tested results of four samples (A-I, A-II, B-I, and B-II)

Table 4 Measured mean thermophysical properties of the samples

Test number	$k \times 10^{-2}$/ Wm^{-1} K^{-1}	$a \times 10^{-7}$/ m^2 s^{-1}	$\rho C \times 10^5$/ J m^{-3} K^{-1}
A-I	6.36	1.46	4.38
A-II	6.26	1.36	4.61
B-I	4.38	1.85	2.38
B-II	4.50	1.95	2.30

Table 5 Thermal properties of each component in samples

Sample component	k/Wm^{-1} K^{-1}	a/m^2 s^{-1}	ρC/Jm^{-3} K^{-1}
Air	0.03	2.48×10^{-5}	1.21×10^3
PET	0.19	1.01×10^{-7}	1.88×10^6

volumetric heat capacity (ρC) grow while the thermal diffusivity (a) reduces.

Conclusions

Three thermophysical properties (k, a, and ρC) of fibrous material are the essential parameters to describe a heat transfer process, noting the interconnections among them through $\rho C = k/a$. An unsteady-state apparatus that can measure/determine these parameters much more quickly is introduced in this paper. Comparing with the steady-state methods and the existing transient methods, it utilizes the stacking and background materials to decrease the interferences of potential local heat convection in porous media and the contact thermal resistance during measurement. Since the Sp numbers for most fibrous materials are around 1.1×10^3–1.25×10^5, such that heat transfer in such porous materials usually takes place at LTE condition and the experimental temperature distributions in both solid (T_s) and fluid (T_f) phases can be treated as equal. We then developed a theoretical model to analyze the heat source effect and the heat loss at the boundaries. By setting up an allowable error limit, we defined a confidence time region ($t_{min} \sim t_{max}$): the influence due to different heat source capacities can be ignored if the measuring time is greater than $t_{min,}$ and the heat loss via outside surface becomes negligible if the testing duration is below t_{max}. It is also established in this work that $t_{min} \sim t_{max}$ is around 30–210 s for most fibrous materials. Four kinds of polyester nonwovens were collected for testing by this apparatus and good repeatability was achieved. The experimental data agreed well with the theoretical predictions. Our results also confirmed the critical role the material density plays in determining the thermal behavior of porous materials.

References

1. Pan N. Modified analysis of the microstructural characteristics of general fiber assemblies. Text Res J. 1993;63(6):336–45.
2. Carnaby GA, Pan N. Theory of the compression hysteresis of fibrous assemblies. Text Res J. 1989;59(5):275–84.
3. Wang M, Pan N. Predictions of effective physical properties of complex multiphase materials. Mater Sci Eng R. 2008;63(1):1–30.
4. Zhu F, Li K. Determining effective thermal conductivity of fabrics by using fractal method. Int J Thermophys. 2010;1–8.
5. Yang H, Zhu S, Pan N. Studying the mechanisms of titanium dioxide as ultraviolet-blocking additive for films and fabrics by an improved scheme. J Appl Polym Sci. 2004;92(5):3201–10.
6. Yang H, Zhu S, Pan N. On the Kubelka-Munk single-constant/two-constant theories. Text Res J. 2010;80(3):263–70.
7. Xin W, Weilin X, Wenbin L, Weigang C. Study on the electrical resistance of textiles under wet conditions. Text Res J. 2009;79(8):753–60.
8. Pan N, He J, Yu J. Fibrous Materials as Soft Matter. Text Res J. 2007;77(4):205–13.
9. Wang M, Pan N. Modeling and prediction of the effective thermal conductivity of random open-cell porous foams. Int J Heat Mass Trans. 2008;51(5–6):1325–31. doi:10.1016/j.ijheatmasstransfer.2007.11.031.
10. Zhmakin LI, Kozyrev IV, Kirokosyan KA. Study of the thermal conductivity of textiles for firefighters' uniforms. Fibre Chem. 2006;38(2):118–20.
11. Vrana T, Gudmundsson K. Comparison of fibrous insulations—cellulose and stone wool in terms of moisture properties resulting from condensation and ice formation. Construct Build Mater. 2010;24(7):1151–7.
12. Amiri A, Vafai K. Analysis of dispersion effects and non-thermal equilibrium, non-Darcian, variable porosity incompressible flow through porous media. Int J Heat Mass Trans. 1994;37(6):939–54.
13. Amiri A, Vafai K. Transient analysis of incompressible flow through a packed bed. Int J Heat Mass Trans. 1998;41(24):4259–79.
14. Minkowycz WJ, Haji-Sheikh A, Vafai K. On departure from local thermal equilibrium in porous media due to a rapidly changing heat source: the Sparrow number. Int J Heat Mass Trans. 1999;42(18):3373–85.
15. Tzou DY. A unified field approach for heat conduction from macro- to micro-scales. J Heat Trans. 1995;117(1):8–16.
16. Vadasz P. Explicit conditions for local thermal equilibrium in porous media heat conduction. Transp Porous Med. 2005;59(3):341–55.
17. Vadasz P. On the paradox of heat conduction in porous media subject to lack of local thermal equilibrium. Int J Heat Mass Trans. 2007;50(21–22):4131–40.
18. Wang L, Wei X. Equivalence between dual-phase-lagging and two-phase-system heat conduction processes. Int J Heat Mass Trans. 2008;51(7–8):1751–6.
19. Salmon D. Thermal conductivity of insulations using guarded hot plates, including recent developments and sources of reference materials. Meas Sci Technol. 2001;12(12):R89–98.
20. Zhu F, Zhang W. Measuring the thermal conductive property of protective fabrics to radiant heat exposure. J Ind Text. 2007;37(2):175–86.
21. Vozár L. A computer-controlled apparatus for thermal conductivity measurement by the transient hot wire method. J Therm Anal Calorim. 1996;46(2):495–505. doi:10.1007/bf02135027.
22. Soliman L, Wasfi M, Hendia T. Thermal properties of polycrystalline ZnIn2Se4. J Therm Anal Calorim. 2000;59(3):971–6. doi:10.1023/a:1010194829872.
23. Shinzato K, Baba T. A laser flash apparatus for thermal diffusivity and specific heat capacity measurements. J Therm Anal Calorim. 2001;64(1):413–22. doi:10.1023/a:1011594609521.
24. Gaal P, Thermitus MA, Stroe D. Thermal conductivity measurements using the flash method. J Therm Anal Calorim. 2004;78(1):185–9. doi:10.1023/b:jtan.0000042166.64587.33.
25. Jirsak O, Gok T, Ozipek B, Pan N. Comparing dynamic and static methods for measuring thermal conductive properties of textiles. Text Res J. 1998;68(1):47–56.
26. C177-04 AS. Standard test method for steady-state heat flux measurements and thermal transmission properties by means of the guarded-hot-plate apparatus. Philadelphia: ASTM; 2004.
27. Zhao CY, Lu TJ, Hodson HP, Jackson JD. The temperature dependence of effective thermal conductivity of open-celled steel alloy foams. Mater Sci Eng. 2004;367:123–31.

28. Hammerschmidt U. A new pulse hot strip sensor for measuring thermal conductivity and thermal diffusivity of solids. Int J Thermophys. 2003;24(3):675.
29. Kubičár L, Bohac V. A step-wise method for measuring thermophysical parameters of materials. Meas Sci Technol. 2000;11:252–8.
30. Lei Z, Zhu SK, Pan N. Transient methods of thermal properties measurement on fibrous materials. J Heat Trans Trans ASME. 2010;132(3). doi:10.1115/1.4000049.
31. Lei Z, Zhu S, Pan N. Determination of sample size for step-wise transient thermal tests. Polym Test. 2009;28(3):307–14.
32. Glatzmaier GC, Fred Ramirez W. Use of volume averaging for the modeling of thermal properties of porous materials. Chem Eng Sci. 1988;43(12):3157–69.
33. Čulík F, Baník I. Determination of temperature field created by planar heat source in a solid body consisting of three parts in mutual thermal contact. Int J Therm Sci. 2009;48(1):204–8.
34. Tye RP, Kubicar L, Lockmuller N. The development of a standard for contact transient methods of measurement of thermophysical properties. Int J Thermophys. 2005;26(6):1917–38.
35. Nnanna AGA, Haji-Sheikh A, Harris KT. Experimental study of non-fourier thermal response in porous media. J Porous Med. 2005;8(1):31–44.
36. Holman JP. Heat transfer. New York: McGraw-Hill; 2009.
37. Weidong Y, Caiyuan C. Textile physics. Shanghai: Donghua University; 2002.
38. Patanaik A, Anandjiwala R. Some studies on water permeability of nonwoven fabrics. Text Res J. 2009;79(2):147–53.
39. Kubicar L, Bohac V, Vretenar V, editors. Thermophysical parameters of phenolic foam measured by the pulse transient method: methodology for low thermal conductivity materials the 27th international thermal conductivity conference (ITCC). Lancaster: DEStech Publication; 2005.
40. Kim KJ, King WP. Thermal conduction between a heated microcantilever and a surrounding air environment. Appl Therm Eng. 2009;29(8–9):1631–41.
41. Matweb. In: Overview of materials for polyethylene terephthalate (PET), unreinforced. 3, 2. 2010. http://www.matweb.com. Accessed 06 July 2010.